

Geophysically constrained inversions of glacier bed topography

Resume of an USRA project

Alexi Morin

August 25, 2020

1 Introduction

1.1 Motivation

Inferring glacier thickness has been a long-standing problem for glaciologist. Determining mean ice thickness lets us estimate the total volume of ice in a given glacier, necessary to quantify the water stored. In the context of climate change, a proper estimate of ice thickness is necessary for correctly estimating sea-level change (e.g. [Farinotti et al., 2016](#)). Many techniques have been developed for this problem, such as *power laws* or *scaling methods*, deriving total ice volume from glacier surface area (e.g. [Bahr et al., 2015](#)). However, the development of more precise runoff projections (e.g. [Ramsankaran et al., 2018](#)) and glacier flow models (e.g. [Werder et al., 2020](#)) is asking for distributed ice thickness information.

Acquiring such data today is often done with a sled-mounted or airborne ground penetrating radar (GPR). While airborne surveys are very effective on ice caps and ice sheets, the complications following the processing of the data in mountainous areas poses another difficulty. Furthermore, ground based surveys can be a very challenging feat as traversing highly crevassed areas is on its own complicated let alone while hauling heavy equipment. (e.g. [Colombero et al., 2019](#)) Those ground surveys can then often leave out vast unmeasured areas, forcing the scientist to extrapolate the acquired data.

These reasons motivate the development of physical and statistical ice thickness inference models.

These methods, using theoretical and mathematical models, often rely on assumptions such as uniform basal shear stress and require additional information such as an estimation of basal velocity (e.g. Farinotti et al., 2016). The number of models is rapidly increasing, hence the need for evaluations of their performance under various conditions. The Ice Thickness Models Intercomparison eXperiment (e.g. Farinotti et al., 2016) *ITMIX* called for a total of 17 models applied to 21 study sites. This study was the basis for the development of a global estimate of distributed glacier thickness (e.g. Farinotti et al., 2019). The five best performing models from the experiment needing easily available satellite data were used to make this worldwide estimation. The model outputs are freely available online for glaciers included in the Randolph Glacier Inventory (e.g. Pfeffer et al., 2014).

The first objective of this project is to assess the accuracy of the ice thickness distribution inferred from Farinotti et al. (2019) and other available models at five study sites of interest to the SFU Glaciology Group. As there is little GPR coverage for our two main study sites, the models will also be compared for two other sites where the bed topography is better known. The second objective is to produce an improved model of the ice-thickness distributions based on the comparison of the *ITMIX* output and various models and in-situ ice-thickness measurements. The different methods explored by Farinotti et al. in *ITMIX* are detailed and information about the necessary data for every method is presented. A review of every study sites explored in this project is presented, followed by the assessment of the error in the consensus estimate(e.g. Farinotti et al., 2019) and other models by comparing them to in-situ data.

2 Background

2.1 *ITMIX*

The Ice Thickness Models Intercomparison eXperiment (Farinotti et al., 2016) is a project launched by the Working Group on Glacier Ice Thickness Estimation, part of the International Association of Cryospheric Sci-

ences (IACS). The experiment consists of 17 different models tested over 21 cases. Every glacier in the comparison however had at least:

- a glacier outline (**GO**)
- a digital elevation model (**DEM**)

And a combination of:

- the surface mass balance (**SMB**)
- the velocity field (\vec{V})
- the rate of ice thickness change ($\frac{\partial h}{\partial t}$)

Four main types of models were outlined throughout the experiment, each needing specific data.

- Minimization approaches
 - Those models defines ice thickness inversion as a minimization problem. They use a cost function consisting of minimizing the difference between observed and modelled data.
- Mass conserving approaches
 - These methods are based on the principle of mass conservation [Farinotti et al. \(2016\)](#) The ice flux divergence $\nabla \cdot q$ has to be compensated by the rate of ice thickness change $\frac{\partial h}{\partial t}$ and the climatic mass balance \dot{b} :
$$\nabla \cdot q = \frac{\partial h}{\partial t} - \dot{b}, \quad (1)$$
- Shear-stress based approaches
 - Those approaches rely on some estimation of the basal shear stress τ . They then solve for the ice thickness h using the shallow ice approximation (Fowler and Larson, 1978)

$$h = \frac{\tau}{f \rho g \sin \alpha} \quad (2)$$

where ρ is the ice density, g is the gravitational acceleration, α the slope angle and f is a friction coefficient.

- Velocity-based approaches
 - The models described in this category are based on a form of Glen's flow law (e.g. [Glen, 1958](#)) and an approximation of either the basal velocity u_b or the depth-averaged velocity \bar{u} from the surface velocity u_s .
- Other approaches
 - GCneuralnet([Clarke et al., 2009](#)) is a model based on artificial neural networks. It is based on the assumption that the subglacial topography resembles nearby unglacierized valleys.
 - The method from Brinkerhoff ([Brinkerhoff et al., 2016](#)) is based on Bayesian inference. The idea is that the bed elevation and the ice flux divergence can be described as Gaussian random fields with known covariance but unknown mean.

The requirements of each of the main mode types are shown in table 1.

Table 1: Models compared in *ITMIX*. A checkmark with an asterix means that the model can make use of the data but it is not needed. Note that the table indicates the needs of the majority in the models presented, some models in the category use more or less data than shown in the table. Further information is shown in [Farinotti et al. \(2016\)](#).

Model	GO	DEM	SMB	\vec{V}	$\frac{\partial h}{\partial t}$
Minimization approach	✓	✓	✓	✓*	
Mass conservation approaches	✓	✓			
Shear-stress based approaches	✓	✓			
Velocity based approaches	✓	✓		✓	
GCneuralnet	✓	✓			
Brinkerhoff	✓	✓	✓	✓	✓

ITMIX ranked the models from best to worst according to four error metrics:

- Average
- Median

- Interquartile range
- 95% confidence interval

and over two rankings:

- Their performance over the glaciers tested by every model. Here the models are compared only by the error metrics on the individual test cases.
- Their performance over all the glaciers. Here the models are penalised for a smaller number of cases tested.

One of the main conclusions from *ITMIX* is that the models needing more sophisticated data, such as the velocity fields \vec{V} , surface mass balance SMB or $\frac{\partial h}{\partial t}$ do not necessarily yield a better model. The inconsistencies between the available datasets, often acquired using different methodologies appears to be the cause ([Farinotti et al., 2016](#)). As there are limited data available for our study sites, it is important to choose a model corresponding to potentially available data for our study cases. The findings of *ITMIX* confirms that the lack of \vec{V} or $\frac{\partial h}{\partial t}$ data should not gravely impact the inferring process for our test cases if such data was not available.

3 Study sites

3.1 North Glacier

3.1.1 Site description

North Glacier, located in the St. Elias mountains, was extensively studied by Flowers and her team between (???). This relatively small glacier, spanning 6.9 km^2 , is well known, with a GPR coverage of 4.89 km^2 (Figure 1)¹. Many data sets are available for this glacier, making it a great tool for testing techniques.

¹GPR coverage polygons were computed as the intersection of the glacier's outline and the convex hull delimited by the GPR point data

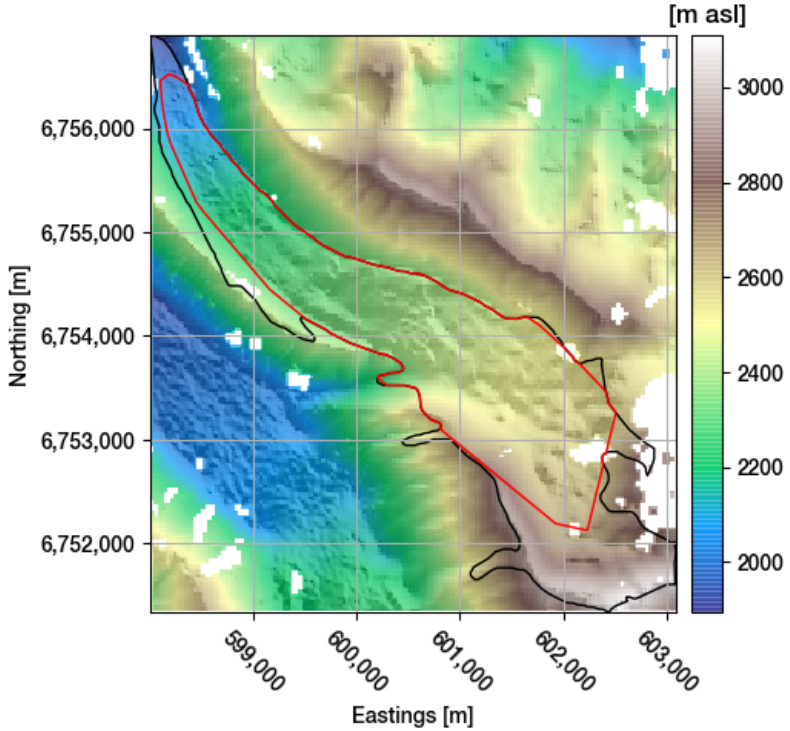


Figure 1: Surface elevation (Need etienne citation) of North Glacier and surroundings with coverage of ice-penetrating radar measurements (red outline). Black outline from [Pfeffer et al. \(2014\)](#)

3.1.2 Data available

Surface elevation data available for this glacier are two 20 m resolution DEM from [Berthier & Toutin \(2008\)](#) and (Need citation from Etienne, see july 10 email), with time-scales representing 2007 and 2018 respectively. From this data was produced a surface elevation change raster, with the same 20 m resolution. 240 m resolution surface velocities from 1985 to 2018 are available from [ITS_LIVE](#) (e.g. [Gardner et al., 2019](#)) and 20 m resolution surface velocities from 2018 are available from (Need etienne's citation). Finally, ice thickness measurements from 2008 are available.

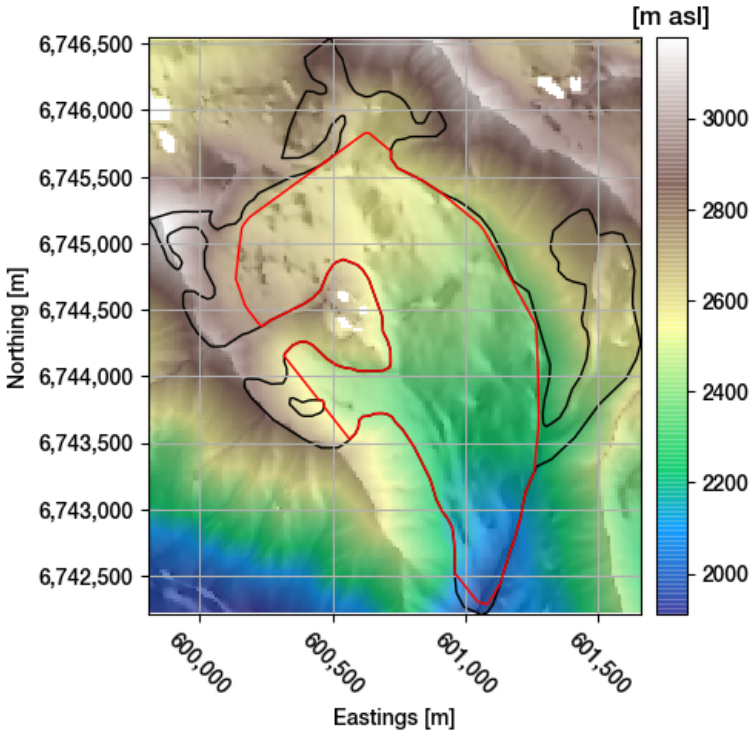


Figure 2: Surface elevation (Need etienne citation) of South Glacier and surroundings with coverage of ice-penetrating radar measurements (red outline). Black outline from [Pfeffer et al. \(2014\)](#)

3.2 South Glacier

3.2.1 Site description

South Glacier was also extensively studied in the same period as North Glacier's. This smaller 5.65 km^2 glacier shows a great GPR coverage of 3.81 km^2 ([3](#))

3.2.2 Data available

Apart from the GPR measurements, 20 m resolution data DEM and surface velocities from 2018 (Need étienne citation) are available.

3.3 Kaskawulsh Glacier

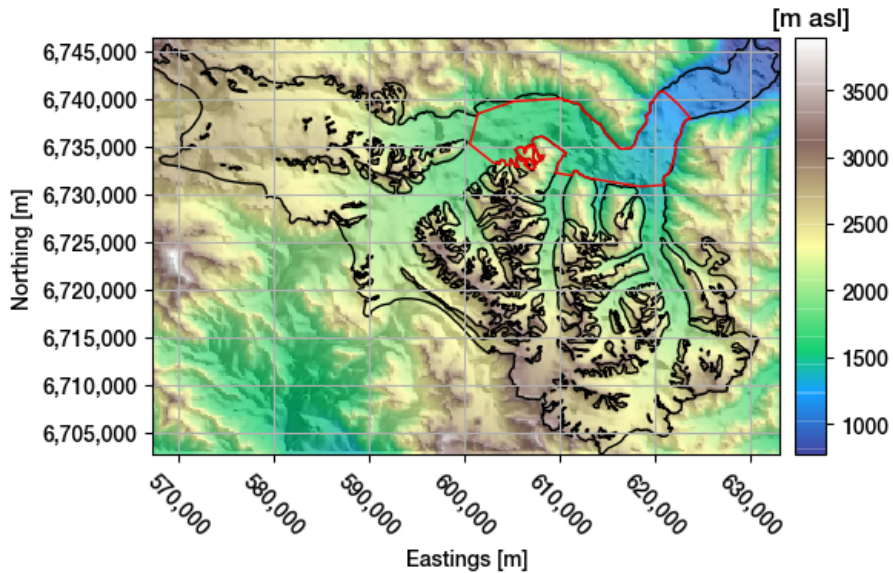


Figure 3: Surface elevation ([Farinotti et al., 2019](#)) of Kaskawulsh Glacier and surroundings with coverage of ice-penetrating radar measurements (red outline). Black outline from [Pfeffer et al. \(2014\)](#)

3.3.1 Site description

Kaskawulsh Glacier is a considerably large glacier of 1053.16 km^2 in the St. Elias mountains. This glacier was studied by Ph.D. student Erik Young as part of a mass balance research project. GPR transects were acquired during the summers of 2018 and 2019, covering approximately 127.84 km^2 .

3.3.2 Data available

Ask Erik about the DEMs used for this particular glacier. None were really used in the process however. More work here is needed.

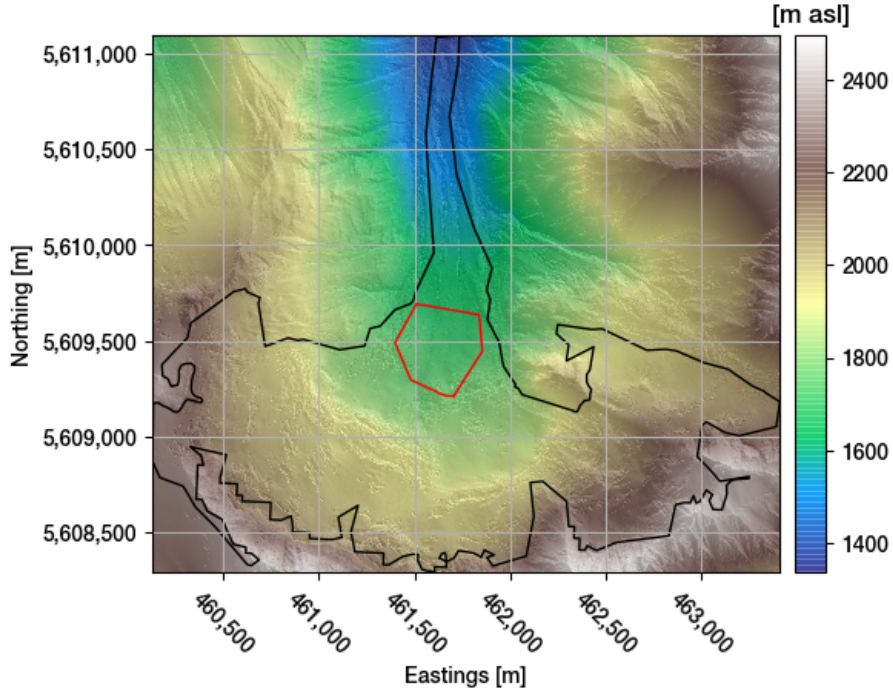


Figure 4: Surface elevation of Job Glacier from [Roberti et al. \(2018\)](#) and surroundings with coverage of ice-penetrating radar measurements (red outline). Black outline from [Pfeffer et al. \(2014\)](#)

3.4 Job Glacier

3.4.1 Site description

Job Glacier is a 3 km long glacier covering $\sim 3 \text{ km}^2$ located in the Mt. Meager complex, a volcano in southwestern British Columbia. This glacier, like most glaciers across the world, has seen a net negative mass balance in the last ten years ([Reyes & Clague, 2004](#)). Fumaroles emerged from the surface of the glacier in 2016. [Roberti et al. \(2018\)](#) states that the fumarolic activity has probably been active for a long period, but only recorded from the thinning of the glacier. MSc research being undertaken by Tryggvi Unnsteinsson aims to understand the dynamical interaction between the glaciological and volcanic systems upon Mt. Meager and the glaciological conditions required for fumarole emergence.

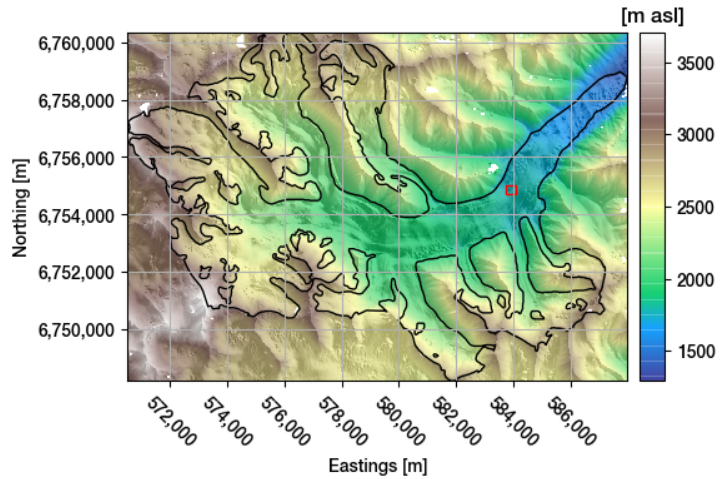
3.4.2 Data available

The data available for this study site consists of a 1 m^2 resolution LIDAR from [Roberti et al. \(2018\)](#), a glacier outline from [Pfeffer et al. \(2014\)](#) and ice thickness measurements from a ground penetrating radar campaign held by Dr. Flowers and her team in September 2018. The ice thickness measurements however only cover a small portion of the glacier, of around 0.15 km^2 , as shown on Figure 4.

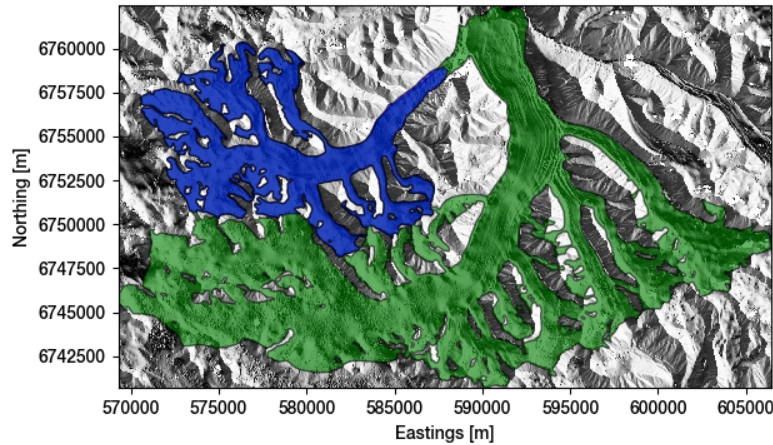
3.5 Little Kluane Glacier

3.5.1 Site description

The little Kluane glacier is the nickname given to a 20 km long glacier covering $\sim 75\text{ km}^2$, part of the bigger Kluane glacier (Figure 5b), located in the St. Elias mountains of Yukon. This glacier has been known to have surged from 2017 to 2018, showing an advance of 1.9 km ([Main et al., 2019](#)). Master's student Andrew Nolan's research aims to understand the impact of climatic changes on surges dynamics.



(a) Surface elevation of little Kluane glacier and surroundings with coverage of ice-penetrating radar measurements (red outline). Black outline from Pfeffer et al. (2014)



(b) Contours from Pfeffer et al. (2014) of little (blue) and big (green) Kluane glaciers.

Figure 5: Elevation and location of the little Kluane glacier in the St. Elias mountains

3.5.2 Data available

The data available consists of two main different data sets with different time-scales which are before and during the end of the glacier's surge.

The pre-surge data, from 2007, consists of a 20 m resolution DEM from [Berthier & Toutin \(2008\)](#), 240 m resolution surface velocities from [ITS_LIVE](#) (e.g. [Gardner et al., 2019](#)) and a glacier outline delimited by Andrew Nolan. The post-surge data, from 2018 to 2019, consists of a 20 m resolution DEM from (Need citation from Étienne, see july 10 email), 240 m resolution surface velocities from [ITS_LIVE](#) (e.g. [Gardner et al., 2019](#)) and a glacier outline also delimited by Andrew Nolan.

Also available is elevation change from 2007 to 2018, an 11 year time-scale. Ice thickness measurements from a GPR survey. Those measurements cover a very small area of the glacier (Figure 5a) of around 0.03 km².

4 The global consensus estimate: assessing the error

Some wonky inconsistencies with the 4-panels figures, need to figure out a consistent way to plot them

Following *ITMIX*, [Farinotti et al. \(2019\)](#) bettered the earlier global estimate from [Huss & Farinotti 2012](#). Findings from *ITMIX* were used to infer ice thickness of all the glaciers around the globe, using five different models and weighting each of their results to minimize the error. The computed models are [available online](#). The increasing availability of globally produced datasets raises the need to acknowledge their quality as they are expected to be used in modelling specific glacier dynamics. Real ice thickness measurements can help us better the approximation made by [Farinotti et al. \(2019\)](#). First, we need to assess the model's error by comparing it to our point data. For h' and h , the modelled and measured thickness values, we can compute the error

$$\Delta h = h' - h \tag{3}$$

by transforming our GPR point data to cell data, the format in which the model is computed. As there are more than one point by cell, the mean value of the point thickness data is taken for each grid cell according to the model's

resolution. From equation 3, positive values of Δh imply *overestimation* of ice thickness from the model and negative values imply *underestimation*.

4.1 North Glacier

The modelled distributed ice thickness (Figure 6a) from Farinotti et al. (2019) for North Glacier seems to respect the measured data, however noting a general trend of overestimating, as seen on Figures 6b and 6d.

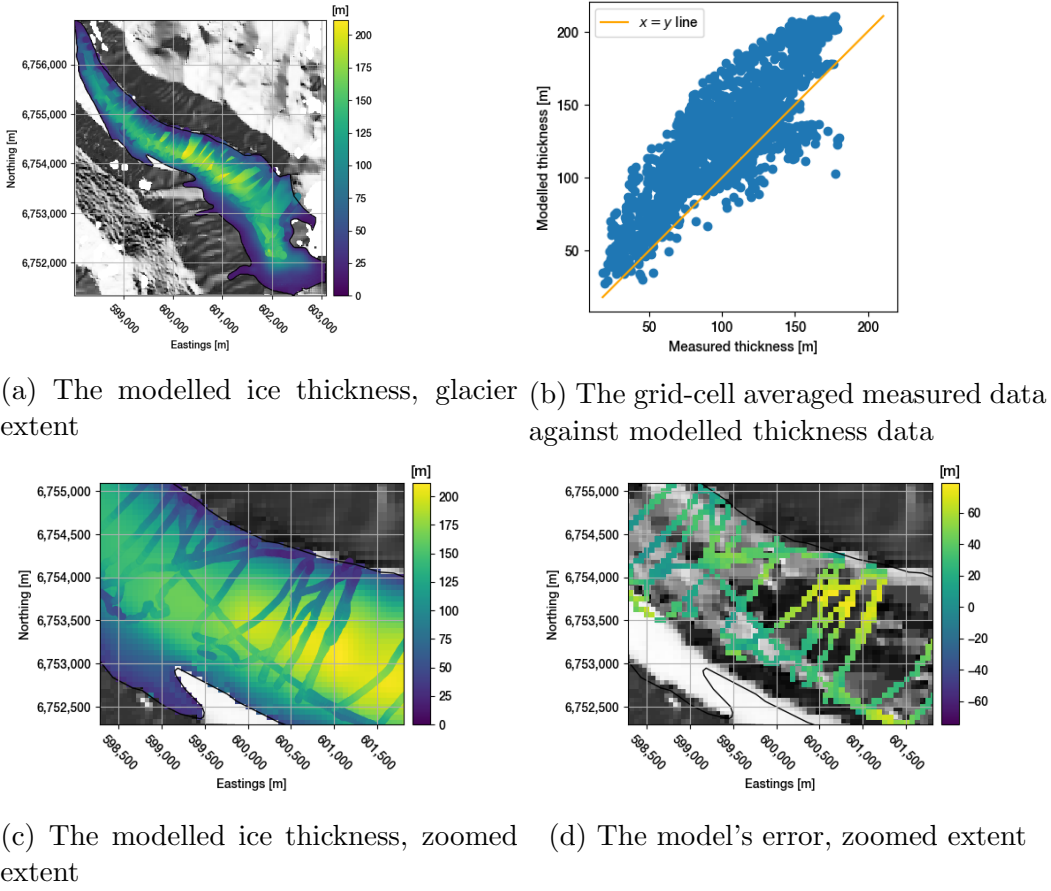
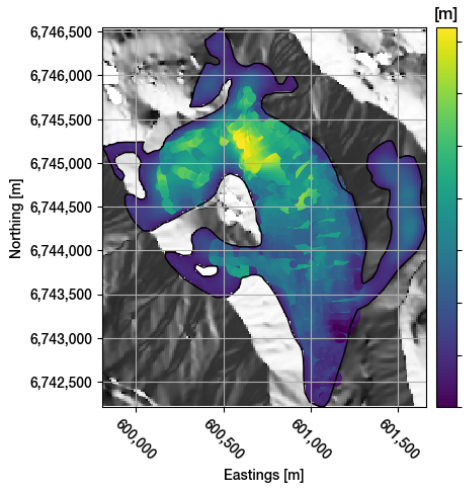


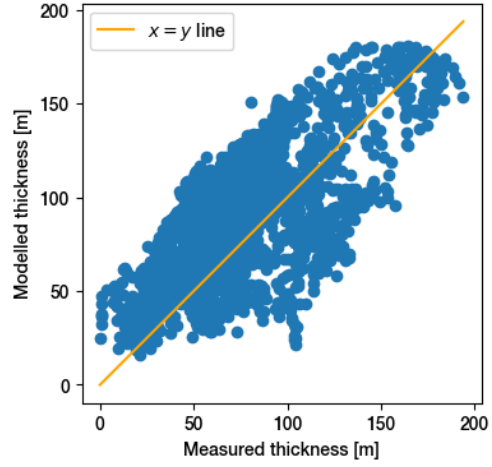
Figure 6: Modelled thickness for North glacier (Farinotti et al., 2019). Points shown on Figures 6a and 6c are thickness measurements from the GPR survey.

4.2 South Glacier

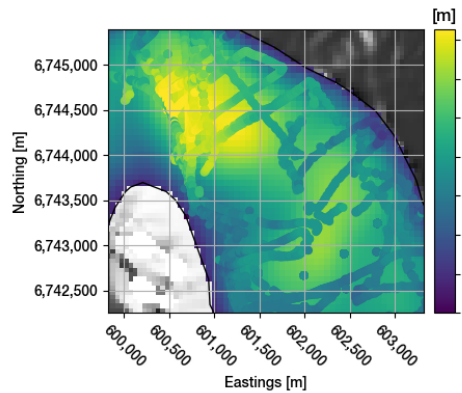
The modelled distributed ice thickness (Figure 6a) from Farinotti et al. (2019) for South Glacier seems to respect the measured data, with no striking trend of either over or under estimating, as seen on Figures 6b and 6d.



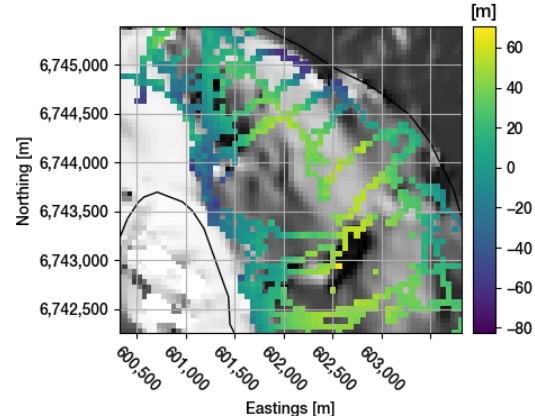
(a) The modelled ice thickness, glacier extent



(b) The grid-cell averaged measured data against modelled thickness data



(c) The modelled ice thickness, zoomed extent



(d) The model's error, zoomed extent

Figure 7: Modelled thickness for South glacier (Farinotti et al., 2019). Points shown on 7a and 7c are thickness measurements from the GPR survey.

4.3 Kaskawulsh Glacier

The vast Kaskawulsh Glacier sees modelled ice thickness (Farinotti et al., 2019) ranging from 0 to 800 meters (Figure 8a). The model correctly guesses the maximum thickness values but overestimates the thinner ice measurements (Figures 8b and 8d).

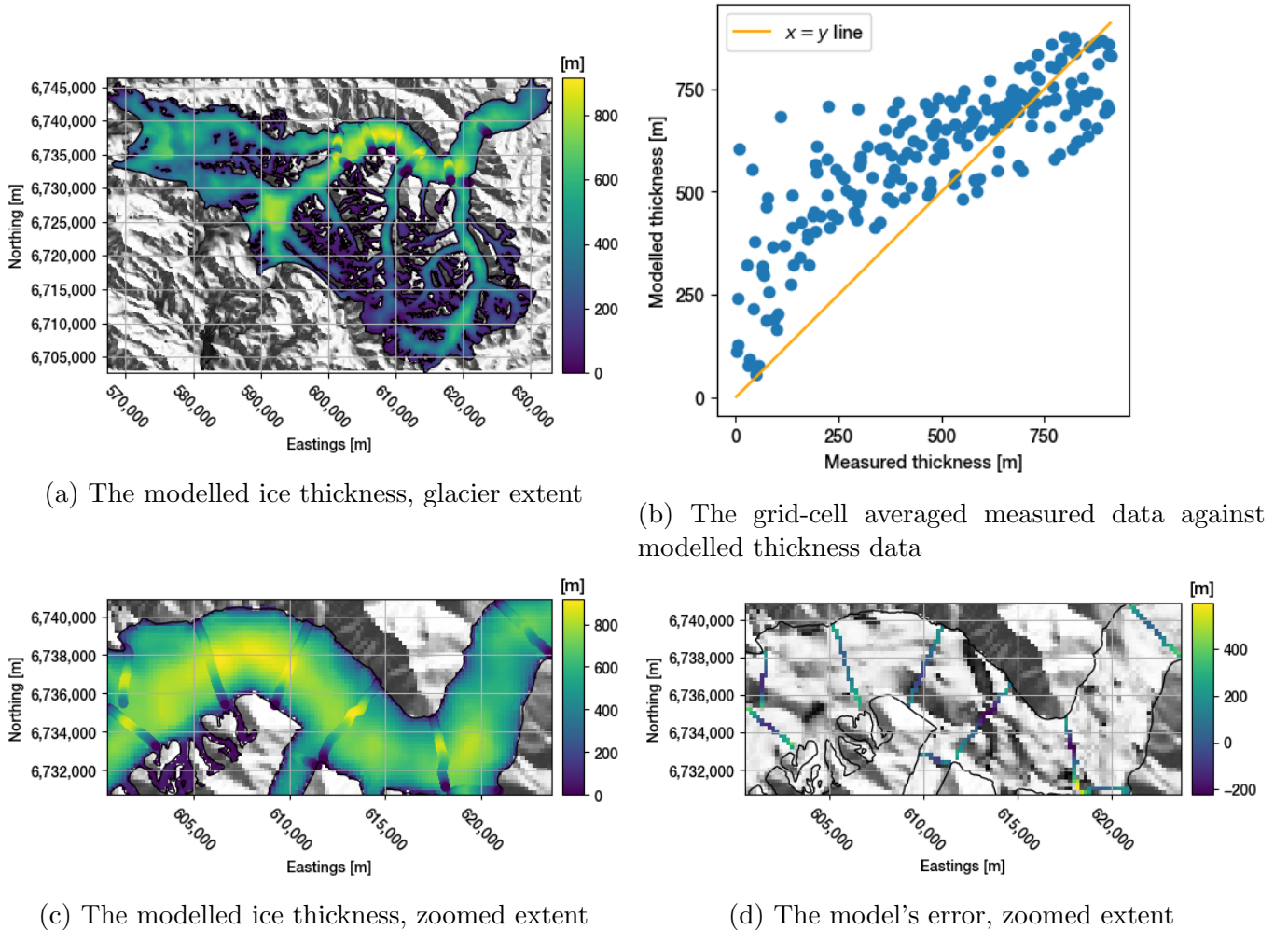


Figure 8: Modelled thickness for South glacier (Farinotti et al., 2019). Points shown on 8a and 8c are thickness measurements from the GPR survey.

4.4 Job Glacier

The modelled distributed ice thickness (Figure 9a) from Farinotti et al. (2019) puts the thinner ice upon the higher elevations and the thicker ice in the lower areas, all the way down the terminus of the glacier. Also shown on Figure 9a is the area covered by the GPR point data. A closer look of the model (Figure 9c) can show us the discrepancies between the modelled and measured data. The larger errors are located upon the margins of the glaciers, modelling thicker and thinner ice to the western and eastern margin respectively (Figure 9d). The measured and modelled ice thickness is plotted on Figure 9b. The higher errors from the models are for larger values of ice thickness, therefore underestimating the glacier's bed topography.

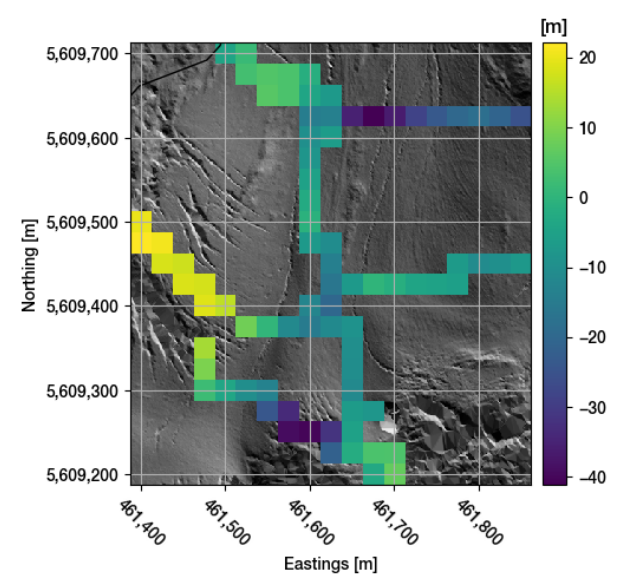
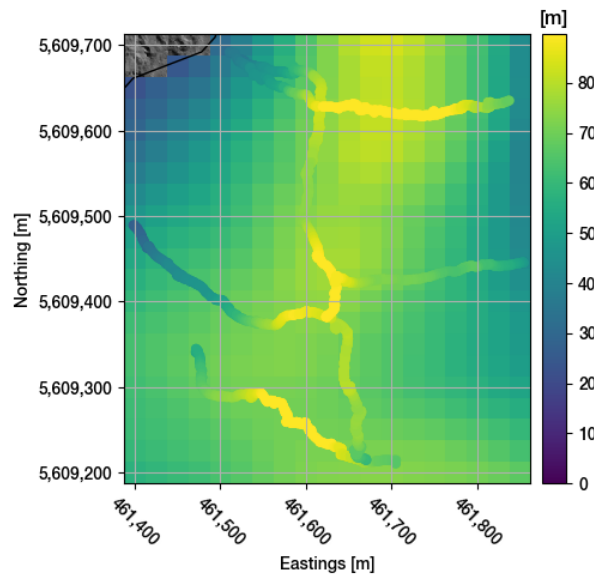
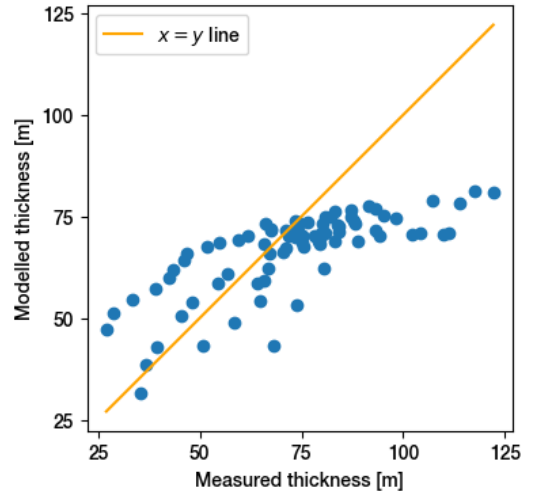
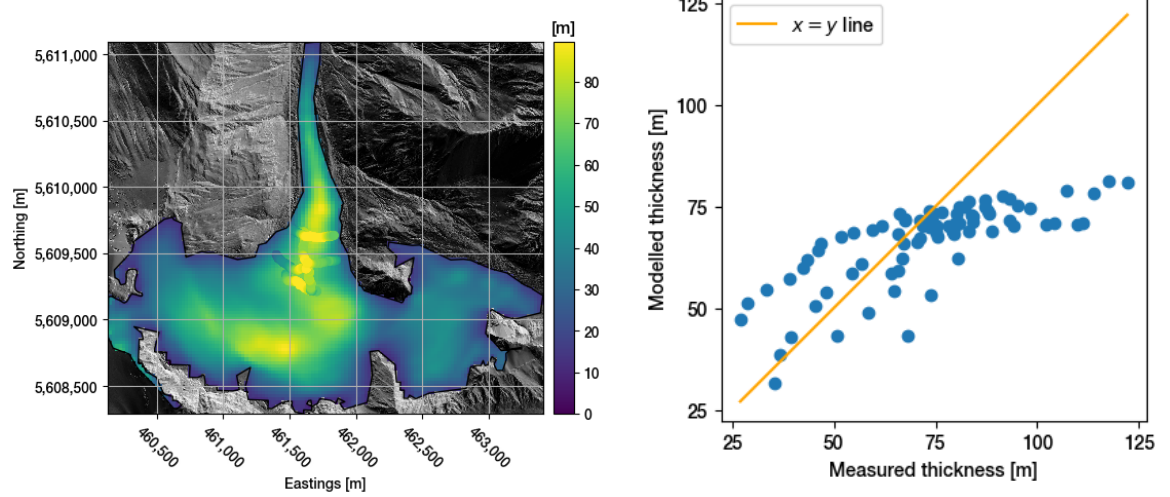


Figure 9: Modelled thickness for Job glacier (Farinotti et al., 2019). Points shown on 9a and 9c are thickness measurements from the GPR survey.

4.5 Little Kluane Glacier

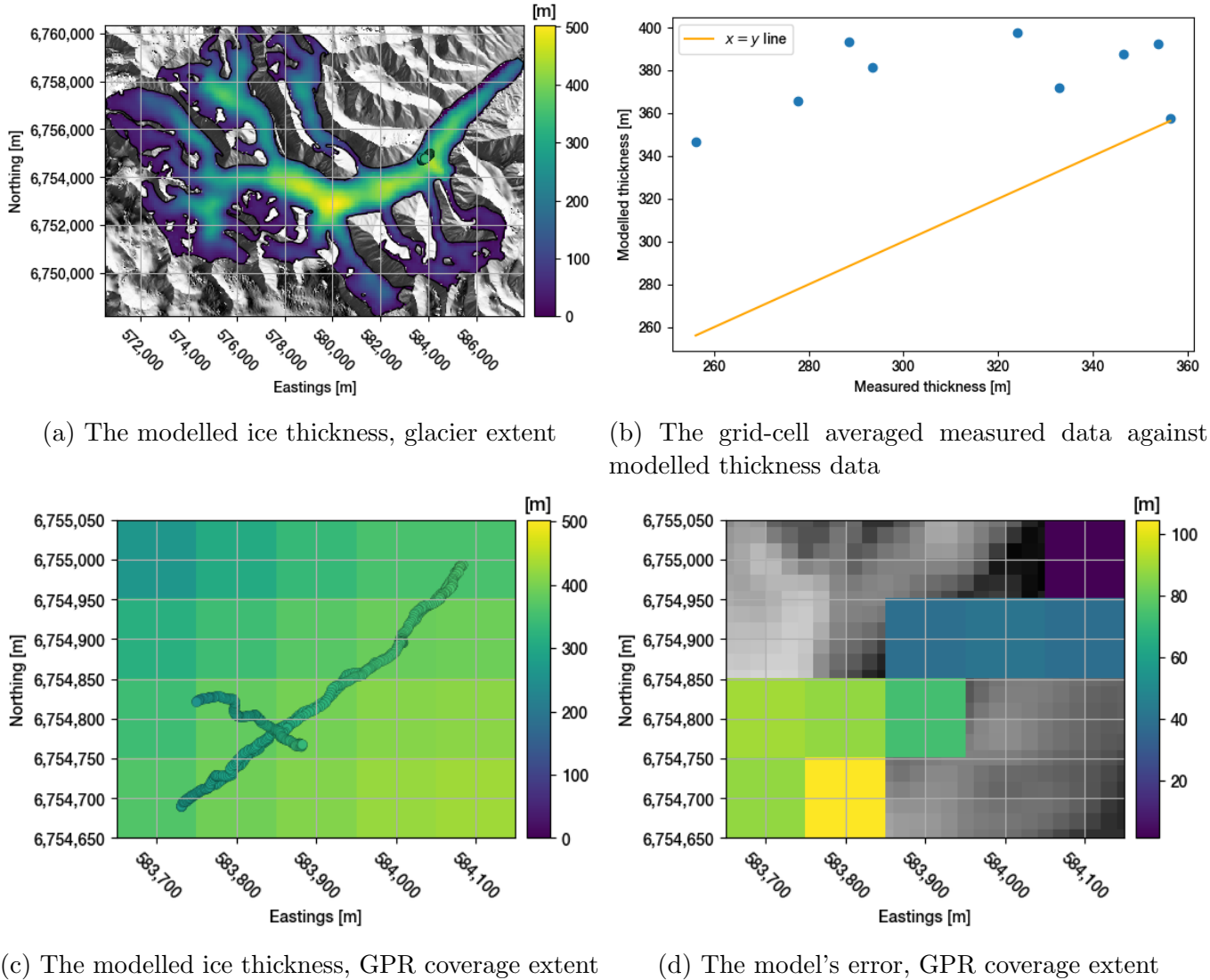


Figure 10: Modelled thickness for little Kluane glacier ([Farinotti et al., 2019](#)). Points shown on 10a and 10c are thickness measurements from the GPR survey.

Little Kluane being a much bigger glacier than Job, the absolute thickness is much greater. The modelled distributed thickness puts the thicker ice in

the lower areas. Because the data was acquired during the surge, covering a great section without having to cross crevasses is a difficult task, hence the smaller GPR coverage (Figure 10c). The produced error-map (Figure 10d) has so few cells that its analysis gives little insight into the model’s representation. However, it is showing errors of up to a 100 m. The model is strictly overestimating the glacier’s thickness (Figure 10b). The time-scales of the model produced by Farinotti et al. (2019) are not available (Farinotti, 2020, personal communication). However, we suspect that based on the timing of the work, the data used is pre-surge. The strict over-estimation of the model is then surprising; one would expect the ice to be thicker after surging, especially down-glacier, where the measurements are coming from.

4.6 Error quantification

By comparing the values from the model's cells and the cell averaged GPR data, we can compute the error Δh according to equation 3. It is always good to first look at the error histograms as they can tell us a lot about the general distribution:

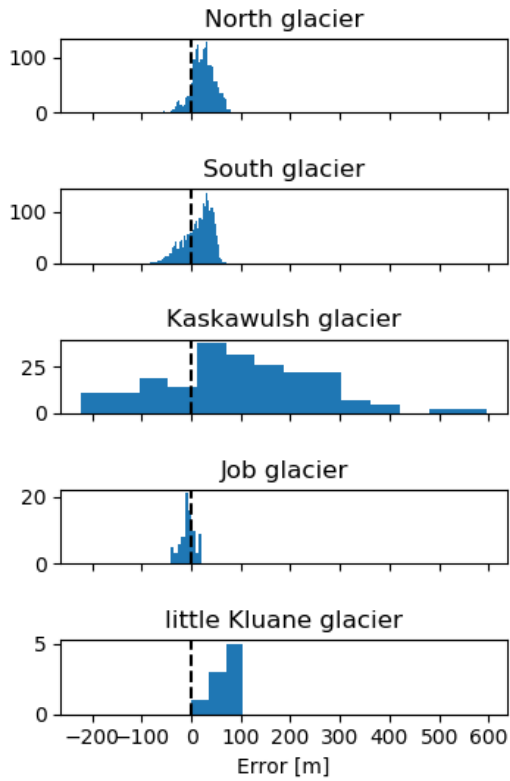


Figure 11: Error distribution from [Farinotti et al. \(2019\)](#) for the different test cases

The histograms of North and South glacier are both slightly asymmetrical and showing a non-zero mode, hence generally overestimating the ice thickness. Those two cases have finer histograms from a much greater number of observed cells to compare data from. The Kaskawulsh Glacier's histogram is also asymmetrical and generally showing ice thickness overestimation. However, it is also showing much greater standard deviation, with errors ranging

from -200 m to 600 m. This is probably due to the impressive scale difference from Kaskawulsh and other test cases. Job Glacier is the only case where the model from Farinotti et al. (2019) is generally underestimating the ice thickness, showing a mode slightly under zero. The Little Kluane Glacier is also showing non-zero mean and mode although the very small number of cells make the histogram's analysis difficult.

Different error metrics can be computed, such as the mean, the standard deviation, the median. Other interesting metrics are the mean absolute error MAE , defined as:

$$MAE = \frac{1}{n} \sum_{i=0}^n |\Delta h_i| \quad (4)$$

where n is the number of cell averaged ice thickness measurements. The MAE tells us about the absolute deviation from zero, giving us an idea of the scale of the general error, omitting the sign. Also interesting to compute is the root mean square error $RMSE$:

$$RMSE = \sqrt{\frac{1}{n} \sum_{i=0}^n (\Delta h_i)^2} \quad (5)$$

In $RMSE$'s case, the higher error values have more weight, resulting in a greater $RMSE$. The different error metrics are shown on Table 2.

Table 2: Error from the ice thickness models computed by Farinotti et al. (2019) for the glacier test cases against cell averaged GPR measurements. Note that every metric is shown in metres.

Glacier	Mean	Std	Median	Max	Min	MAE	RMSE
North glacier	24.16	22.58	24.61	78.86	-75.03	27.82	33.07
South glacier	14.18	28.11	20.63	70.46	-82.78	27.30	31.48
Kaskawulsh glacier	99.31	155.11	94.34	595.68	-221.59	147.54	184.18
Job glacier	-6.62	14.74	-6.62	22.13	-41.13	12.67	16.16
little Kluane glacier	62.79	32.16	73.71	104.73	1.34	62.79	70.55

The different error metrics seems to be correlated with the scale of the glacier, with smaller errors from Job Glacier, to North and South Glaciers, Little Kluane and finally Kaskawulsh glacier. It is then difficult to compare the different computed error metrics and really capture any general trend.

However, Table 2’s data can confirm that the only generally underestimated ice thickness is in Job Glacier’s case. To take care of the different scales, we can take a look at the relative error:

$$\delta h = \frac{\Delta h}{h} \quad (6)$$

This error however is problematic for very small or null values of h , lending to unreasonably large or non numeric mean values. However, we can still try to compute the same metrics and see what they look like (Table 3).

Table 3: Relative error from the ice thickness models computed by [Farinotti et al. \(2019\)](#) for the glacier test cases against cell averaged GPR measurements. Note that every metric is shown in percentages.

Glacier	Mean	Std	Median	Max	Min	MAE	RMSE
North glacier	30.74	31.93	23.56	205.26	-42.15	33.47	44.32
South glacier	inf	nan	31.53	inf	-79.35	inf	inf
Kaskawulsh glacier	169.56	800.80	18.43	7417.17	-26.12	175.58	818.55
Job glacier	-3.58	23.50	-8.66	76.49	-36.74	18.12	23.77
little Kluane glacier	21.22	12.17	22.75	36.31	0.38	21.22	24.46

South and Kaskawulsh’s glaciers error metrics are either non numeric or still disproportionate. We can avoid this problem by omitting smaller thickness values, setting an arbitrary acceptance threshold. By only comparing the relative error for $h \geq 5$ m, we get this table:

Table 4: Relative error from the ice thickness models computed by [Farinotti et al. \(2019\)](#) for the glacier test cases against cell averaged GPR measurements. Note that every metric is shown in percentages. Every value of $h < 5$ m was omitted.

Glacier	Mean	Std	Median	Max	Min	MAE	RMSE
North glacier	30.74	31.93	23.56	205.26	-42.15	33.47	44.32
South glacier	33.43	57.27	31.25	604.83	-79.35	46.76	66.31
Kaskawulsh glacier	112.76	539.05	18.30	7190.90	-26.12	118.84	550.72
Job glacier	-3.58	23.50	-8.66	76.49	-36.74	18.12	23.77
little Kluane glacier	21.22	12.17	22.75	36.31	0.38	21.22	24.46

The relative error for South Glacier now looks more like North Glacier, which is to be expected, as they have both similar geographical localisations

and GPR coverage. However, Kaskawulsh Glacier's relative error is lower, but not to more acceptable levels. With a mean absolute relative error of 112.76 %, the estimate from Farinotti et al. (2019) is on average either twice or half the measured value. Job Glacier and Little Kluane glaciers show a good fit with the observed data, with a mean relative error of -3.58 % and 21.22 %. However, the differences between the GPR coverage for every glacier is important (see Table 5)

Table 5: Relative GPR coverage for the different glaciers. The relative coverage is the coverage area (Figure ??) divided by the glacier's area from Pfeffer et al. (2014).

Glacier	Relative GPR coverage [%]
North glacier	70.96
South glacier	67.34
Kaskawulsh glacier	12.14
Job glacier	4.90
little Kluane glacier	0.04

In North and South glacier's cases, the error analysis is probably telling us valid information about the mode as the GPR coverage is over 50 %. It is not clear, however, for Kaskawulsh Glacier: even if the computed relative coverage is of 12.14 %, the actual coverage is probably smaller given the geometry of the transects (Figure 8c). The computed error metrics are nonetheless not convincing of a good fit. For Job and Little Kluane glaciers, the error analysis is not sufficient to tell if the model computed by Farinotti et al. (2019) is good or not given the poor GPR coverage of less than 5 % for both glaciers. Furthermore, the comparison of the model for little Kluane glacier is not coherent given that the ice thickness model was computed using pre-surge data for a much bigger glacier (Figure 5b) and that the GPR measurements were taken during the surge.

It is then particularly important for the multiple reasons above to at least try to better the available bed models from ? or even infer the bed topography from data in which we are confident in the time-scales.



Figure 12: The intersection of the glacier’s outline and the convex hull formed by the GPR points is the GPR coverage area. Showcased here is North Glacier’s.

5 GlaTe model

5.1 The full GlaTe algorithm

The freely available online GlaTe model (e.g. [Langhammer et al., 2019](#)) aims to, using surface elevation, a glacier outline and ice thickness measurements, minimize the discrepancy between modelled and observed data.

The GlaTe model initially estimates the distributed ice thickness \hat{h}^{glac} using a physical model inspired by [Clarke et al. \(2013\)](#). This physical model takes as input a DEM and a glacier outline. With this available ice thickness data h^{GPR} , the algorithm reduces the observable error on this approximation by scaling the physical model \hat{h}^{glac} by a coefficient α_{GPR} from minimizing a cost function q defined as

$$q = \|h^{GPR} - \alpha_{GPR}\hat{h}^{glac}\|^2 \quad (7)$$

which is equivalent of a linear regression with a fixed (and null) intercept. This coefficient is used such that

$$h^{glac} = \alpha_{GPR}\hat{h}^{glac} \quad (8)$$

is a supposedly better overall approximation, giving a bigger weight to the observed data and minimizing the impact of generalized trends in the physical model. Using this better approximation h^{glac} , the algorithm aims to solve this system of equations:

$$\begin{bmatrix} \lambda_1 \mathbf{G} \\ \lambda_2 \mathbf{L} \\ \lambda_3 \mathbf{B} \\ \lambda_4 \mathbf{S} \end{bmatrix} h^{est} = \begin{bmatrix} \lambda_1 h^{GPR} \\ \lambda_2 \nabla h^{glac} \\ 0 \\ 0 \end{bmatrix} \quad (9)$$

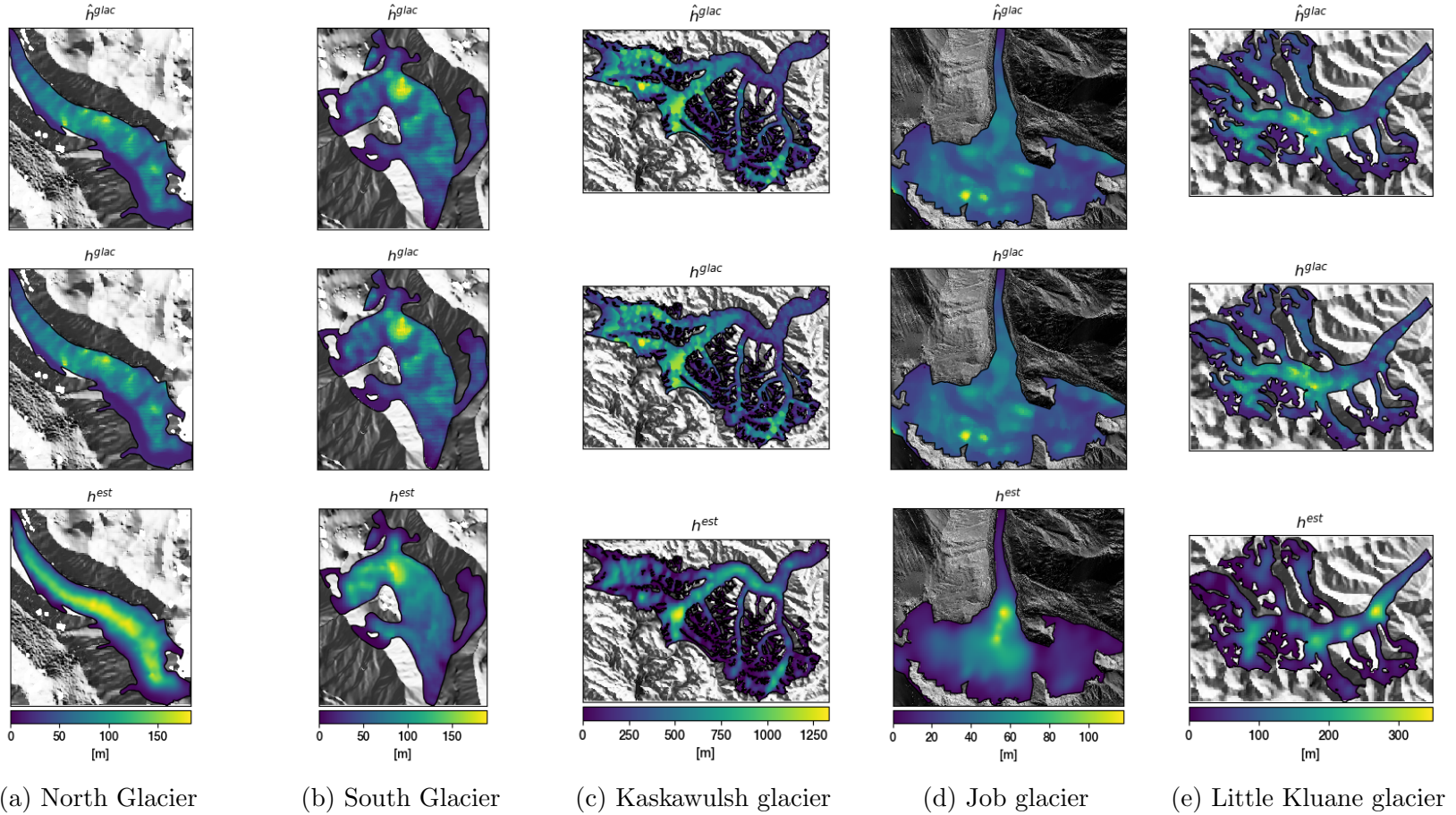
where :

- h^{est} is the modelled ice thickness distribution
- $\lambda_1 \mathbf{G}$ are used to fit the observed data within uncertainty
- $\lambda_2 \mathbf{L}$ are used to avoid systematic differences between observed and modelled data
- $\lambda_3 \mathbf{B}$ are used to ensure zero thickness at the boundaries
- $\lambda_4 \mathbf{S}$ are used to obtain a smoother surface, as \mathbf{S} is a smoothing matrix.

The scalar values λ_i are respective weights for every equation in the system and are tuned during the algorithm's run until an arbitrary error threshold for h^{est} is met. The GlaTe model could be described as a physical method of ice thickness interpolation. The algorithm thus outputs three distributed ice thickness maps:

- The physical model \hat{h}^{glac}
- The *corrected* or rather scaled physical model $h^{glac} = \alpha_{GPR} \hat{h}^{glac}$
- The final estimation h^{est}

Those can be observed for the test cases (Figure 13) where the GlaTe algorithm was applied. The resulting modelled ice thickness h^{est} shows a very small observable error (Figure 14).



(a) North Glacier (b) South Glacier (c) Kaskawulsh glacier (d) Job glacier (e) Little Kluane glacier

Figure 13: Thickness maps produced with the complete GlaTe algorithm for the test cases. Physical model is inspired from [Clarke et al. \(2013\)](#).

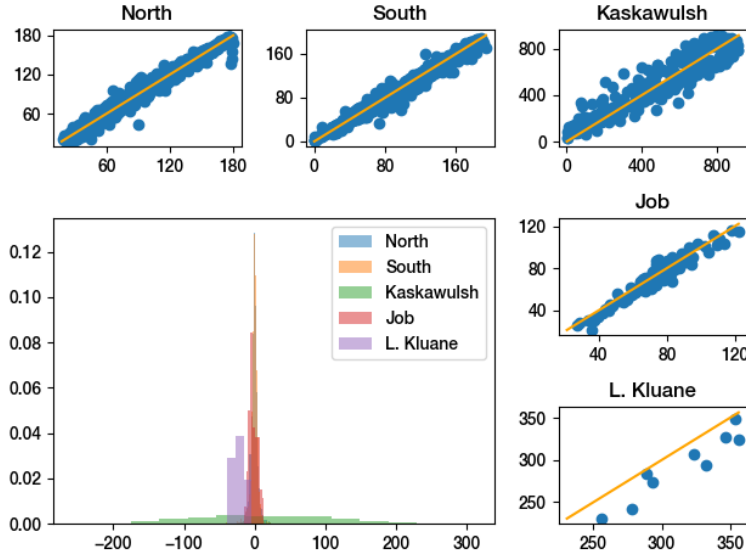


Figure 14: Scatterplot of the measured (x -axis) and modelled h^{est} (y -axis) for the test cases. Bottom left are the normalised h^{est} error [m] histograms of the different test cases. Physical model inspired by [Clarke et al. \(2013\)](#).

Figure 14 gives the impression that the h^{est} model is close to a perfect estimate of the bed ice thickness. However, this is due to the nature of the GlaTe algorithm, reducing the error for known data points only. We cannot assess the validity of a model from observing the error for known data points only, an educated, arbitrary opinion is necessary. When looking at the ice thickness fields produced by the complete GlaTe algorithm for the poorer coverage glaciers (Kaskawulsh, Job and Little Kluane), the thickness maps make little sense:

- Kaskawulsh Glacier's maximum ice thickness (1250 m!) region is located in the upper part of the elevation range
- Job Glacier shows very thin ice almost everywhere
- Little Kluane Glacier shows thick ice at every tributary junction, diminishing in thickness in between

Due to nature of the GlaTe algorithm, there is little physical meaning in the resulting ice thickness field h^{est} . By itself, the GlaTe algorithm uses a

physical model \hat{h}^{glac} inspired by [Clarke et al. \(2013\)](#). By inputting another physical model \hat{h}^{glac} for the rest of the algorithm, perhaps the resulting estimate h^{est} will be better (Figure 16)? Once again, the resulting observable error from h^{est} is very good (Figure 15). The error shows a very small standard deviation and is centred around zero for most of the cases. However, a few things can tell us that the resulting h^{est} model is not exactly right:

- The resulting plot from using the physical model \hat{h}^{glac} from [Farinotti et al. \(2019\)](#) (Figure 15) is quasi identical to the one produced using the complete GlaTe algorithm and it's physical model from [Clarke et al. \(2013\)](#) (Figure 14). This tells us that h^{est} gives little meaning to the initial physical model for the cells with GPR coverage, resulting in the same data.
- Kaskawulsh, Job and Little Kluane distributed ice thickness fields show very thin ice over almost all of the glaciers.

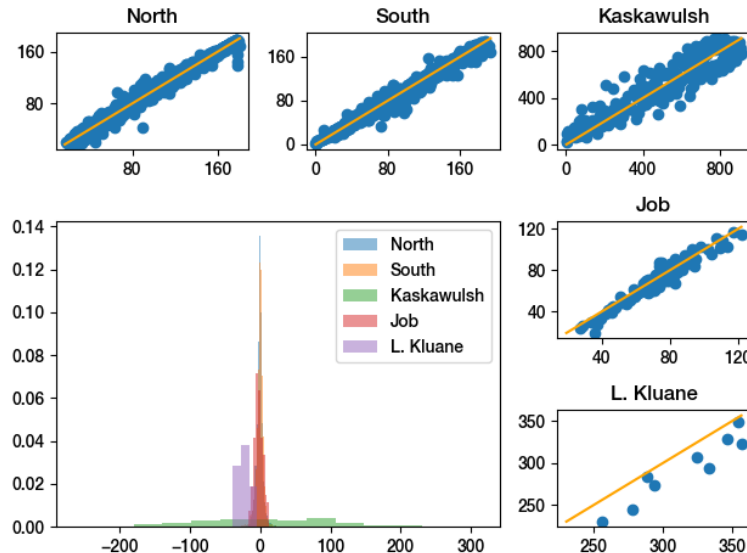


Figure 15: Scatterplot of the measured (x -axis) and modelled h^{est} (y -axis) for the test cases. Bottom left are the normalised h^{est} error [m] histograms of the different test cases. Physical model from [Farinotti et al. \(2019\)](#)

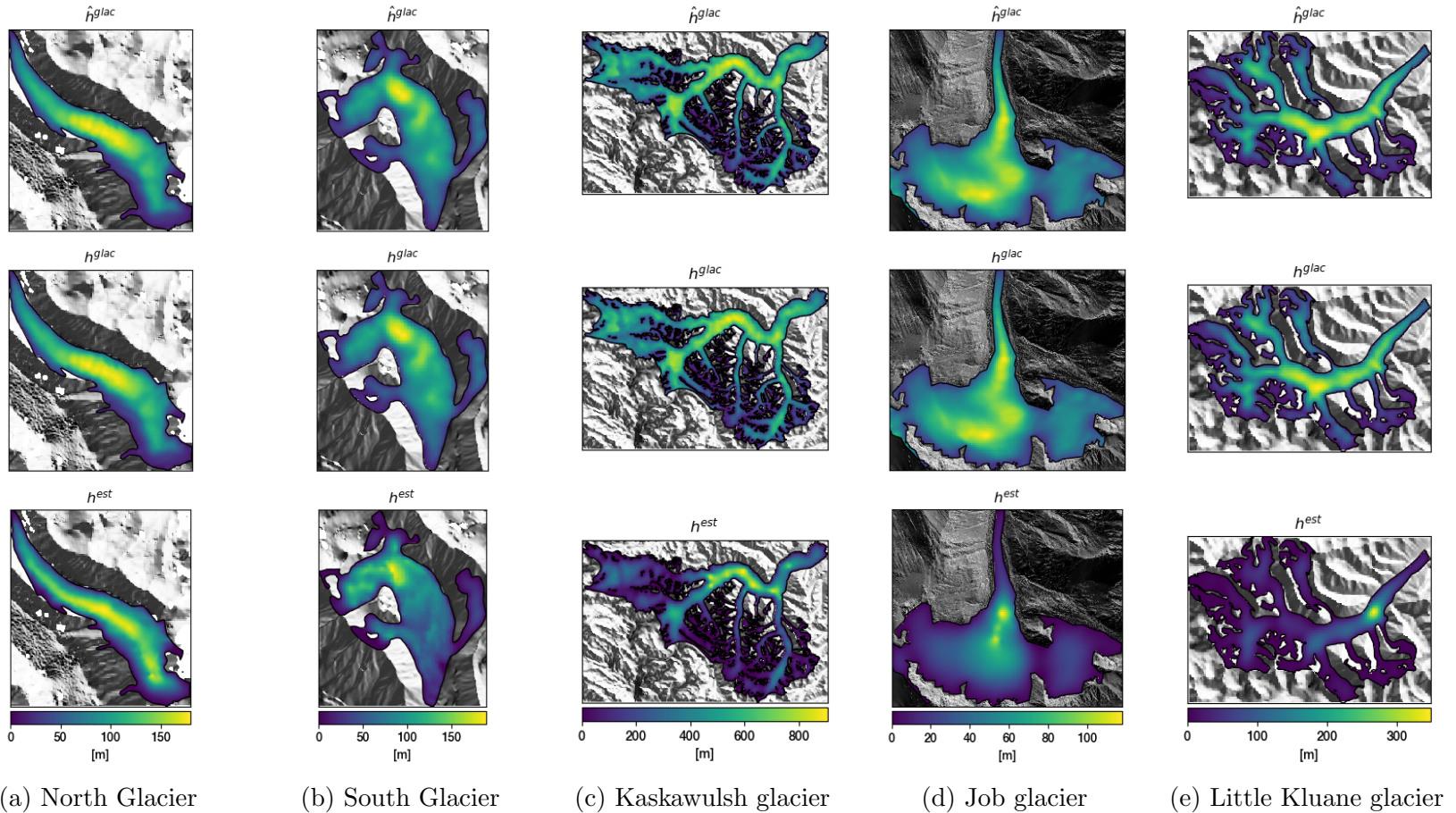


Figure 16: Thickness maps produced with the GlaTe algorithm and \hat{h}^{glac} from Farinotti et al. (2019) for the test cases.

It seems like the GlaTe algorithm does a poor job of modelling distributed ice thickness when the GPR coverage is not all over the glacier. To verify the full GlaTe algorithm's performance over glaciers with worse GPR coverage, a small sample of points on North Glacier was arbitrarily selected and the resulting GPR data was set as input h^{GPR} through the GlaTe algorithm. The resulting model (Figure 17a) was compared against the complete data set. h^{est} ended up, like in the precedent cases, severely underestimating the ice thickness. The scatterplot (Figure 17b) shows that h^{est} only fits the input data, ignoring the rest of the glacier. The entire GlaTe algorithm is then not a good approach to obtain bed topography for our test cases.

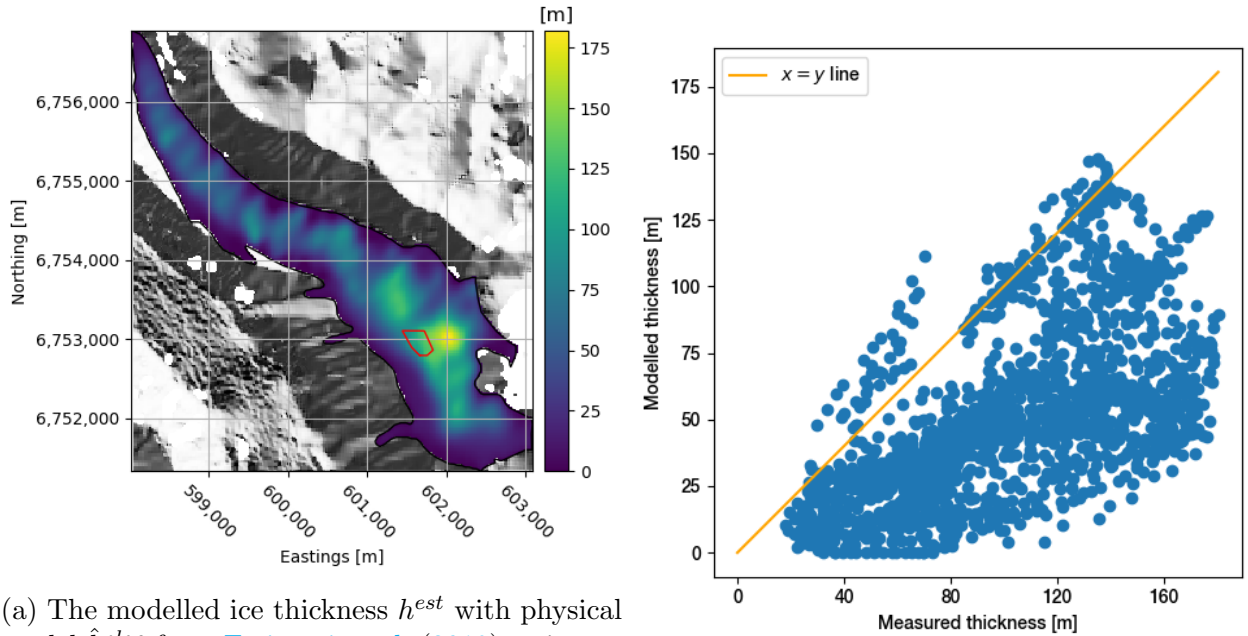


Figure 17: Testing the GlaTe algorithm for North Glacier with only a few GPR points as input data.

5.2 Verifying α_{GPR}

An interesting approach from the GlaTe algorithm is to scale an ice thickness model \hat{h}^{glac} by a scalar α_{GPR} . This scalar, obtained by minimizing the cost function from equation 7, is then used to obtain a *better* approximation following equation 8. To compute this scalar², one needs to:

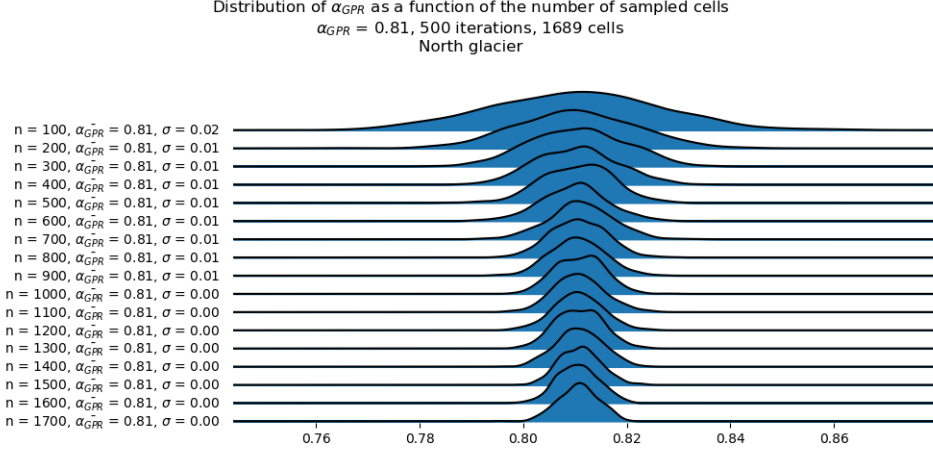
1. Transform the GPR point data to cell data. This is h^{GPR} . This raster needs to be of the same resolution and size as the ice thickness model \hat{h}^{glac} .
2. Compute the coefficient α_{GPR} by minimising the cost function from equation 7. This can be done using your favorite least square method.
3. Multiply the initial \hat{h}^{glac} by the α_{GPR} value obtained at step 2 to obtain h^{glac} .

However, this approach should only better our estimation if a good coverage of the radar data is had, which is not the case for our study sites of Job and little Kluane. We can use our test cases with a better coverage, North and South glacier, to check if the values for α_{GPR} we obtain for an arbitrary number of GPR points resemble the *best* value by considering it to be the one we obtain with our complete GPR data set. By randomly selecting an arbitrary number N of GPR data points, their corresponding modelled cells and computing the equivalent α_{GPR} multiple (many many much) times, we can estimate the distribution of α_{GPR} for N data points³. We see that distribution is strongly centered on the *true* value of α_{GPR} and showing a rather small standard deviation for both cases (Figure 18).

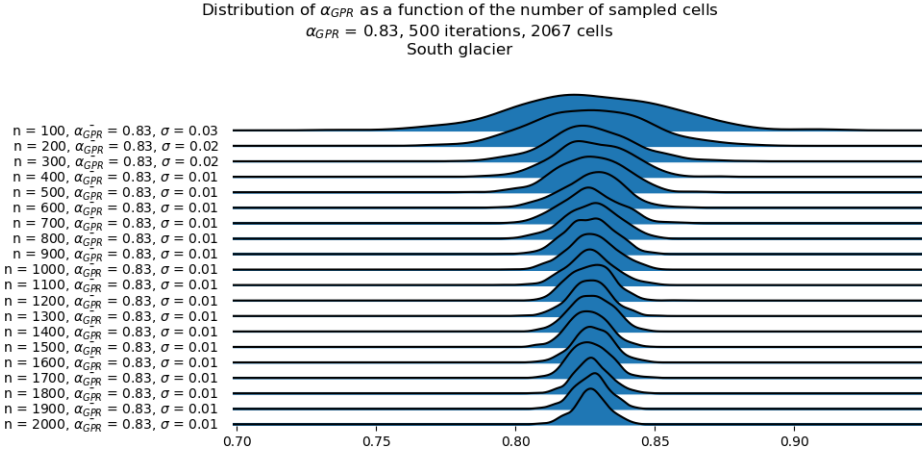
However, to represent the true spatial distribution of our datasets, we need to sample such random data. By randomly selecting one GPR data point and only the nearest cells, we can approximate such a random *clumped* distribution for a more credible case. The distribution is less strongly centred on the *true* value of α_{GPR} for small values of N and shows a much greater standard deviation (Figure 19). The distribution is also strongly bimodal for increasing values of N . This is likely due to the less extreme nature of the

²Or simply [use the pyGM library available on GitHub!](#) More information in the appendix.

³The [code](#) used for this sampling is available on GitHub



(a) North glacier

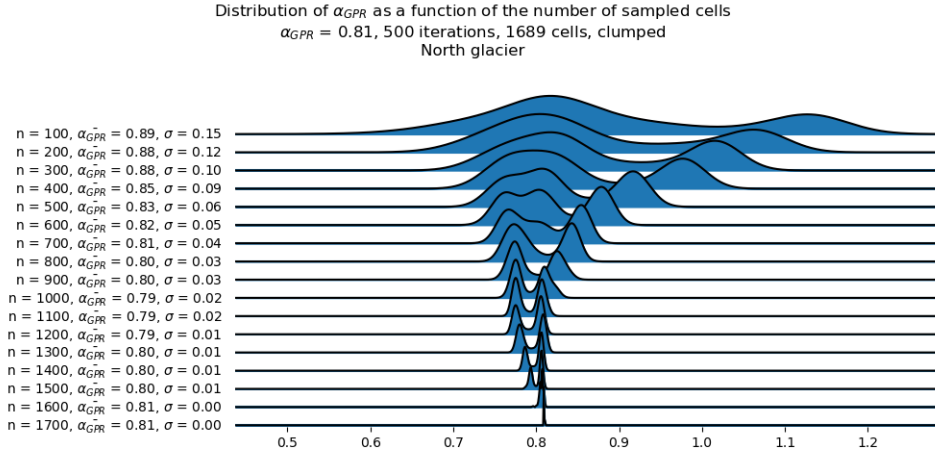


(b) South glacier

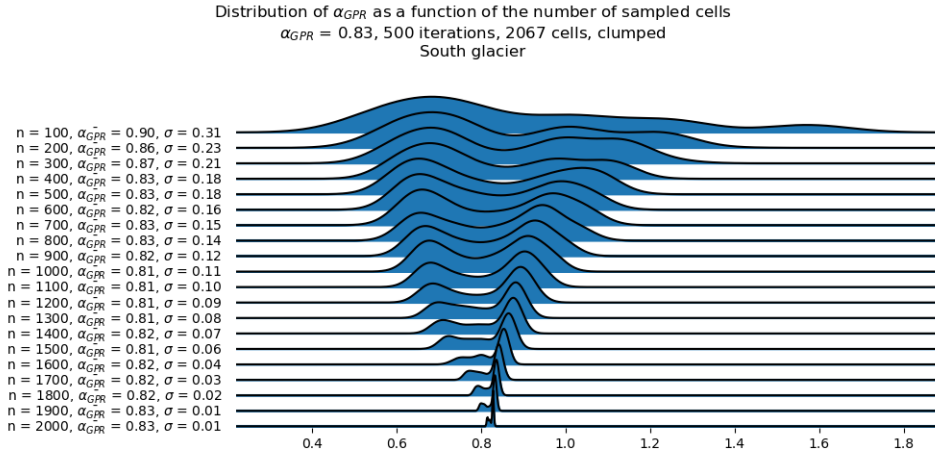
Figure 18: Distribution of α_{GPR} for randomly sampled N cells

models, underestimating and overestimating ice thickness in the lower and higher regions.

For an ice thickness estimate h^{glac} in which one is confident, such as the model from Farinotti et al. (2019), one can scale it by a factor of α_{GPR} computed from equations 7 and 8. This model should be a *better* model following Figure 19.



(a) North glacier



(b) South glacier

Figure 19: Distribution of α_{GPR} for randomly sampled N clumped cells

6 Appendix

6.1 pyGM: Tool for comparing glacier models

I plan to fill this section up when I have the time to do further polishing following Andrew's suggestions. I'd like this section to be a guide on what this library can do.

6.2 The Kaskawulsh glacier

As part of Young et al. (references needed) article about the Kaskawulsh glacier's mass balance, flux gates area were computed. To compute those flux gates, one needs bed topography data, coming from either real world measurements or from inference. Ground penetrating radar data for this particular glacier was collected in the summers of 2018 and 2019. Flux gate area was computed by past undergraduate student Rebecca Latto in the summer of 2019 by summing the ice thickness values multiplied by 10, thus assuming a constant 10 meters distance between the point data.

As part of this ice thickness inference project, the differences between modelled and measured data for the Kaskawulsh glacier was computed. The main goal was to evaluate the potential error that would be made for the flux gate's area if one was to use modelled thickness data. Latto's data was unfortunately not geo-referenced: for a given line, the only information had was that the points were along the line and separated by a constant distance of 10 meters. However, splitting the lines in such a way, using QGIS, did not work as the algorithm ended up outputting more or less points than that of Latto's data. Therefore a 1 to 1 connection could not be established.

What was done was that a given line was split up in as many points as there was thickness data for it. The distances between the points were then computed, resembling more or less 10 meters⁴. Having the (x, y) coordinates meant that it could then be used to compare the measured thickness with models by extracting model values at those (x, y) coordinates (Figures 8c and 8b).

To note is that some problems were had noting the orientation of the data. It was assumed that the transects data was orientated down glacier. This can be a problem when computing the error as the differences between the modelled and the observed data. However, it should not be a major problem when computing the differences between the modelled and measured area of the transects.

To compute the modelled flux gate areas, modelled ice thickness values \hat{h} were extracted at every (x, y) point where there was measured data. The

⁴The code used for this task and the data produced is available on GitHub

distances between the points were computed as

$$d = \sqrt{(x_i - x_{i-1})^2 + (y_i - y_{i-1})^2} \quad (10)$$

and the area was computed using numpy's trapezoid integration (need reference?) algorithm. The [data](#) generated is available on GitHub and visible on Table 6.

Table 6: Gate areas computed from GPR data, [Farinotti et al. \(2019\)](#) and its scaled model.

Gate	h_A^{GPR} [km ²]	\hat{h}_A^{glac} [km ²]	$0.92\hat{h}_A^{glac}$ [km ²]	$\frac{h_A^{GPR} - \hat{h}_A^{glac}}{h_A^{GPR}}$	$\frac{h_A^{GPR} - \hat{h}_A^{glac}}{\hat{h}_A^{glac}}$
CA	1.72	2.11	1.94	-0.23	-0.19
KW1	1.7	2.36	2.17	-0.39	-0.28
KW2	1.93	2.29	2.1	-0.18	-0.15
KW3	2.93	3.05	2.8	-0.04	-0.04
KW4	2.83	3.12	2.86	-0.1	-0.09
KW5	2.52	3.2	2.93	-0.27	-0.21
NA	1.67	1.77	1.62	-0.06	-0.06
SA	1.07	1.42	1.3	-0.32	-0.24
SW	0.63	0.72	0.66	-0.14	-0.12

References

- Bahr, D. B., Pfeffer, W. T., & Kaser, G. (2015). A review of volume-area scaling of glaciers. *Reviews of Geophysics*, 53(1), 95–140.
- Berthier, E., & Toutin, T. (2008). Spot5-hrs digital elevation models and the monitoring of glacier elevation changes in north-west canada and south-east alaska. *Remote Sensing of Environment*, 112(5), 2443–2454.
- Brinkerhoff, D. J., Aschwanden, A., & Truffer, M. (2016). Bayesian inference of subglacial topography using mass conservation. *Frontiers in Earth Science*, 4, 8.
- Clarke, G. K., Anslow, F. S., Jarosch, A. H., Radić, V., Menounos, B., Bolch, T., & Berthier, E. (2013). Ice volume and subglacial topography

- for western canadian glaciers from mass balance fields, thinning rates, and a bed stress model. *Journal of Climate*, 26(12), 4282–4303.
- Clarke, G. K., Berthier, E., Schoof, C. G., & Jarosch, A. H. (2009). Neural networks applied to estimating subglacial topography and glacier volume. *Journal of Climate*, 22(8), 2146–2160.
- Colombero, C., Comina, C., De Toma, E., Franco, D., & Godio, A. (2019). Ice thickness estimation from geophysical investigations on the terminal lobes of belvedere glacier (nw italian alps). *Remote Sensing*, 11(7), 805.
- Farinotti, D., Brinkerhoff, D., Clarke, G. K., Fürst, J. J., Frey, H., Gantayat, P., ... others (2016). How accurate are estimates of glacier ice thickness? results from itmix, the ice thickness models intercomparison experiment. *The Cryosphere Discussions*.
- Farinotti, D., Huss, M., Fürst, J. J., Landmann, J., Machguth, H., Maussion, F., & Pandit, A. (2019). A consensus estimate for the ice thickness distribution of all glaciers on earth. *Nature Geoscience*, 12(3), 168–173.
- Gardner, A., Fahnestock, M., & Scambos, T. (2019). Its_live regional glacier and ice sheet surface velocities. *Data archived at National Snow and Ice Data Center*.
- Glen, J. (1958). The flow law of ice: A discussion of the assumptions made in glacier theory, their experimental foundations and consequences. *IASH Publ*, 47(171), e183.
- Huss, M., & Farinotti, D. (2012). Distributed ice thickness and volume of all glaciers around the globe. *Journal of Geophysical Research: Earth Surface*, 117(F4).
- Langhammer, L., Grab, M., Bauder, A., & Maurer, H. (2019). Glacier thickness estimations of alpine glaciers using data and modeling constraints. *Cryosphere*, 13(8), 2189–2202.
- Main, B., Copland, L., Samsonov, S. V., Dow, C. F., Flowers, G. E., Young, E., & Kochtitzky, W. H. (2019). Surge of little kluane glacier in the st. elias mountains, yukon, canada, from 2017-2018. *AGU FM*, 2019, C31B–1517.

- Pfeffer, W. T., Arendt, A. A., Bliss, A., Bolch, T., Cogley, J. G., Gardner, A. S., ... others (2014). The randolph glacier inventory: a globally complete inventory of glaciers. *Journal of Glaciology*, 60(221), 537–552.
- Ramsankaran, R., Pandit, A., & Azam, M. F. (2018). Spatially distributed ice-thickness modelling for chhota shigri glacier in western himalayas, india. *International Journal of Remote Sensing*, 39(10), 3320–3343.
- Reyes, A. V., & Clague, J. J. (2004). Stratigraphic evidence for multiple holocene advances of lillooet glacier, southern coast mountains, british columbia. *Canadian Journal of Earth Sciences*, 41(8), 903–918.
- Roberti, G., Ward, B., van Wyk de Vries, B., Falorni, G., Menounos, B., Friele, P., ... others (2018). Landslides and glacier retreat at mt. meager volcano: hazard and risk challenges. *GeoHazards 7, Canmore 2018*.
- Werder, M. A., Huss, M., Paul, F., Dehecq, A., & Farinotti, D. (2020). A bayesian ice thickness estimation model for large-scale applications. *Journal of Glaciology*, 66(255), 137–152.